

Non-resonant global mode in LHD partial collapse with net toroidal current

journal or publication title	Nuclear Fusion
volume	61
number	12
page range	126056
year	2021-11-18
NAIS	12971
URL	http://hdl.handle.net/10655/00013087

doi: <https://doi.org/10.1088/1741-4326/ac3292>



PAPER • OPEN ACCESS

Non-resonant global mode in LHD partial collapse with net toroidal current

To cite this article: K. Ichiguchi *et al* 2021 *Nucl. Fusion* **61** 126056

View the [article online](#) for updates and enhancements.

You may also like

- [Enhancement of helium exhaust by resonant magnetic perturbation fields at LHD and TEXTOR](#)
O. Schmitz, K. Ida, M. Kobayashi et al.
- [International Stellarator/Heliotron Database progress on high-beta confinement and operational boundaries](#)
A. Weller, K.Y. Watanabe, S. Sakakibara et al.
- [Observation of carbon impurity flow in the edge stochastic magnetic field layer of Large Helical Device and its impact on the edge impurity control](#)
T. Oishi, S. Morita, S.Y. Dai et al.

Non-resonant global mode in LHD partial collapse with net toroidal current

K. Ichiguchi^{1,2,*} , Y. Suzuki^{1,2,5} , Y. Todo¹ , S. Sakakibara^{1,2}, K. Ida^{1,2} ,
Y. Takemura^{1,2} , M. Sato¹ , L.E. Sugiyama³ and B.A. Carreras⁴ 

¹ National Institute for Fusion Science, Toki, Japan

² The Graduate University for Advanced Studies, SOKENDAI, Toki, Japan

³ Massachusetts Institute of Technology, Cambridge, MA, United States of America

⁴ BACV Solutions Inc., Oak Ridge, TN, United States of America

E-mail: ichiguchi.katsuji@nifs.ac.jp

Received 28 May 2021, revised 30 July 2021

Accepted for publication 22 October 2021

Published 18 November 2021



CrossMark

Abstract

A transition from an interchange mode to a non-resonant mode is found in the nonlinear magnetohydrodynamic simulation for the partial collapse in a large helical device (LHD) plasma with a net toroidal current. This transition can occur when the magnetic shear is weak and the rotational transform is close to unity in the core region. In this transition, the mode number of the dominant Fourier component is reduced. As a result of the nonlinear evolution, the $(m, n) = (1, 1)$ component can be dominant, where m and n are the poloidal and the toroidal mode numbers, respectively. This transition is considered to be a candidate to explain the observation in the LHD experiments with the net toroidal current that show partial collapses are caused by the $(1, 1)$ mode.

Keywords: magnetohydrodynamics (MHD), numerical simulation, non-resonant mode, partial collapse, large helical device (LHD)

(Some figures may appear in colour only in the online journal)

1. Introduction

In the magnetic confinement systems of fusion plasmas such as tokamaks, stellarators and heliotrons, it is crucial that the plasmas are stable against magnetohydrodynamic (MHD) instabilities. Therefore, in the large helical device (LHD) [1], which is the largest heliotron device, the stability performance is extensively studied in the experiments. The heliotron configurations have the great advantage that the confinement magnetic field can be generated by the outer coil system without driving the net toroidal current in the plasma. Because of this advantage, the heliotron plasmas can generally avoid plasma disruption

or significant transients in plasma stored energy by avoiding beta limits and carefully avoiding net toroidal current scenarios. In the LHD experiments, the average beta value of 5% was achieved as the highest value [2].

On the other hand, it is also necessary in the development of the fusion reactor to clarify the stability boundary and the variety of the stability property with respect to the various parameters in the magnetic configuration and the plasma condition. For this purpose, the experiments with the net toroidal current have also been conducted in the LHD experiments [3–6]. In the experiments, the net toroidal current is driven by the neutral beam injection so that the rotational transform t is increased. In this case, partial collapse phenomena are observed when the current reaches a certain value. In the collapses, the electron temperature decreases in the time scale of 100 ms. The profile in the core region is flattened after the collapse, of which the radius of the area is more than half of the plasma minor radius. The axis beta is also decreased by about 60% [3]. Such collapses are not observed in the cases without the net toroidal current for the corresponding conditions.

* Author to whom any correspondence should be addressed.

⁵ Present address: Graduate School of Advanced Science and Engineering, Hiroshima University, Higashi-Hiroshima, Japan.



Original content from this work may be used under the terms of the [Creative Commons Attribution 4.0 licence](https://creativecommons.org/licenses/by/4.0/). Any further distribution of this work must maintain attribution to the author(s) and the title of the work, journal citation and DOI.

One of the specific features in such experiments is that the collapses are always caused by the $(m, n) = (1, 1)$ mode. The profile of the electron temperature during the collapse shows an asymmetric shape corresponding to the $m = 1$ mode. This mode is considered to be the pressure driven mode, in particular, the interchange mode, because the equilibria are strongly Mercier unstable. However, according to the theory of the standard interchange mode, the linear growth rate is larger for higher mode numbers [7]. Therefore, it has been required to explain why the partial collapses are caused by the $(1, 1)$ mode in LHD.

Recently, Sugiyama *et al* discussed the appearance of the $(1, 1)$ mode in the sawtooth crash in the DIII-D tokamak [8]. They examined the crash numerically by means of the M3D code [9, 10] in the situation that the safety factor q , which is the inverse of the rotational transform, is flat and close to unity in the core region. They found that the quasi-interchange mode [11] is destabilized, which causes the crash. This result means that the $(1, 1)$ component in the category of the interchange modes can be dominant in such crashes. On the other hand, in the LHD experiments, the profile of the rotational transform is also considered to be raised up and to be made flat due to the peaked beam current. This situation is similar to the case of the destabilization of the quasi-interchange mode in the DIII-D case. Thus, in this study, we employ the analogy of this sawtooth simulation in the analysis of the problem for the dominant $(1, 1)$ mode appearance in the LHD partial collapses. That is, we numerically study the nonlinear behavior of the LHD plasma with such a rotational transform generated by the net toroidal current by means of the three-dimensional (3D) nonlinear MHD simulations. First, the nonlinear evolution of the interchange mode in the equilibrium *without* the net toroidal current and a high shear is shown as a reference. Then, the result for the equilibrium *with* the net toroidal current and a low shear is discussed.

This paper is composed as follows. In section 2, the numerical method utilized in this study is explained. The equilibria examined here are also shown. In section 3, the example of the typical interchange mode for the equilibrium without the net toroidal current and with a high shear in the substantially Mercier unstable case is described as the reference. In section 4, the nonlinear evolution of the plasma behavior in the case of the low shear by the net toroidal current is discussed. The nonlinear transition to the $(1, 1)$ non-resonant mode is shown. The concluding remarks are given in section 5.

2. Numerical method and equilibrium

In the present numerical simulations, the HINT [12] and the MIPS [13] codes are utilized for the equilibrium and the nonlinear dynamics calculations, respectively. In the HINT code, the 3D equilibrium is obtained without any assumption for the existence of the nested flux surfaces. The equilibrium equations are solved through the iteration of two steps in the cylindrical coordinates (R, ϕ, Z) . In the first step, the pressure P is obtained with the fixed magnetic field \mathbf{B} by solving

$$\mathbf{B} \cdot \nabla P = 0. \quad (1)$$

In the second step, \mathbf{B} is obtained with P fixed in the relaxation process of the two equations,

$$\frac{\partial \mathbf{v}}{\partial t} = -\nabla P + \mathbf{J} \times \mathbf{B} + \hat{\nu} \nabla^2 \mathbf{v}, \quad \frac{\partial \mathbf{B}}{\partial t} = \nabla \times (\mathbf{v} \times \mathbf{B} - \hat{\eta} \mathbf{J}), \quad (2)$$

where $\hat{\nu}$ and $\hat{\eta}$ are artificial parameters for the convergence.

In the equilibrium calculation of this study, the vacuum magnetic configuration of $R_{\text{ax}} = 3.6$ m for the horizontal magnetic axis position and $\gamma_c = 1.1739$ for the helical coil pitch parameter are employed. This configuration corresponds to that in the experiment in reference [3]. The pressure profile P_{eq} is employed as $P_{\text{eq}} = P_0 (1 - 0.68\rho^2 - 0.32\rho^4)$. Here ρ denotes the square root of the normalized toroidal magnetic flux. In the present study, two equilibria are examined. One is the equilibrium without a net toroidal current at $\beta_0 = 3.3\%$ as the reference, where β_0 denotes the axis beta value. This beta value is chosen so that the feature of the typical interchange mode should be emphasized. The other is the equilibrium with a net toroidal current at $\beta_0 = 1.4\%$. In this case, the profile of the current density is assumed as $J_{\text{eq}} = J_0(1 - \rho^2)^4$, and $I/B = 29.6$ kA T⁻¹ is employed for the total current.

Figures 1(a) and (b) show the puncture plots of the field lines of the equilibria in the cases without and with the net toroidal current. No magnetic islands are observed in these plots, while the HINT code can calculate the equilibria involving the islands. Figure 1(c) shows the rotational transform and the Mercier index D_I [14] of these equilibria. The positive and the negative values of D_I mean Mercier unstable and stable situations against the ideal interchange mode, respectively. The rotational transform has a monotonically increasing profile in the equilibrium without the net current case at $\beta_0 = 3.3\%$. On the other hand, in the case with the net toroidal current at $\beta_0 = 1.4\%$, the magnetic shear is very weak in the core region for $\rho < 0.6$. The value of the rotational transform is close to unity in this region and has a minimum $\epsilon = 0.955$ at $\rho = 0.36$. The Mercier indices at the typical resonant surfaces concerned in the later discussions are $D_I = 1.09$ at $\epsilon = 2/3$ for the equilibrium without the net toroidal current and $D_I = 1.41$ at $\epsilon = 1$ for the equilibrium with the net toroidal current. These are significantly large values which indicate that both of these equilibria should be unstable against the ideal interchange modes resonant at these surfaces.

In the MIPS code, the full MHD equations,

$$\frac{\partial \rho_m}{\partial t} = \nabla \cdot (\rho_m \mathbf{v}) + D \nabla^2 (\rho_m - \rho_{\text{meq}}) \quad (3)$$

$$\begin{aligned} \rho_m \frac{\partial \mathbf{v}}{\partial t} &= -\rho_m \boldsymbol{\omega} \times \mathbf{v} - \rho_m \nabla \left(\frac{v^2}{2} \right) - \nabla P + \mathbf{J} \times \mathbf{B} \\ &\quad + \frac{4}{3} \nabla [\nu \rho_m (\nabla \cdot \mathbf{v})] - \nabla \times [\nu \rho_m \boldsymbol{\omega}], \\ \boldsymbol{\omega} &= \nabla \times \mathbf{v} \end{aligned} \quad (4)$$

$$\begin{aligned} \frac{\partial P}{\partial t} &= -\nabla \cdot (P \mathbf{v}) - (\Gamma - 1) P \nabla \cdot \mathbf{v} + \nabla \cdot [\chi_{\perp} \nabla (P - P_{\text{eq}}) \\ &\quad + (\chi_{\parallel} - \chi_{\perp}) (\mathbf{b} \cdot \nabla P) \mathbf{b}] \end{aligned} \quad (5)$$

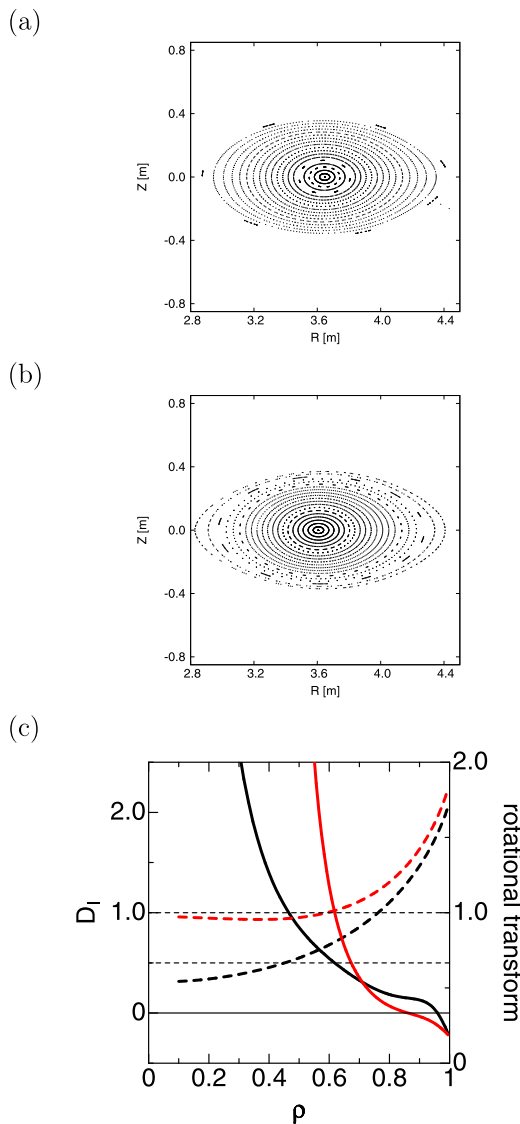


Figure 1. Puncture plots of the field lines of the equilibria for (a) $\beta_0 = 3.3\%$ and $I = 0$ and (b) $\beta_0 = 1.4\%$ and $I/B = 29.6$ kA, and (c) profiles of Mercier index \bar{D}_I (solid lines) and rotational transform (dashed lines) for the $\beta_0 = 3.3\%$ and $I = 0$ equilibrium (black lines) and $\beta_0 = 1.4\%$ and $I/B = 29.6$ kA T^{-1} equilibrium (red lines). The horizontal black dashed lines correspond to $\bar{\tau} = 2/3$ and 1.

$$\frac{\partial \mathbf{B}}{\partial t} = -\nabla \times \mathbf{E}, \quad \mathbf{J} = \frac{1}{\mu_0} \nabla \times \mathbf{B} \quad (6)$$

$$\mathbf{E} = -\mathbf{v} \times \mathbf{B} + \eta(\mathbf{J} - \mathbf{J}_{\text{eq}}) \quad (7)$$

are solved as an initial value problem for mass density ρ_m , fluid velocity \mathbf{v} , pressure P and magnetic field \mathbf{B} . Here \mathbf{b} denotes the unit vector of \mathbf{B} and the subscript ‘eq’ means the equilibrium quantity.

As the numerical scheme, the 4th order finite difference for the spatial discretization and the 4th order Runge–Kutta scheme for the time evolution are employed. The Kawamura–Kuwahara scheme [15] is also applied for the numerical stability. In the nonlinear dynamics calculation, the equilibrium mass density is assumed to be constant and normalized

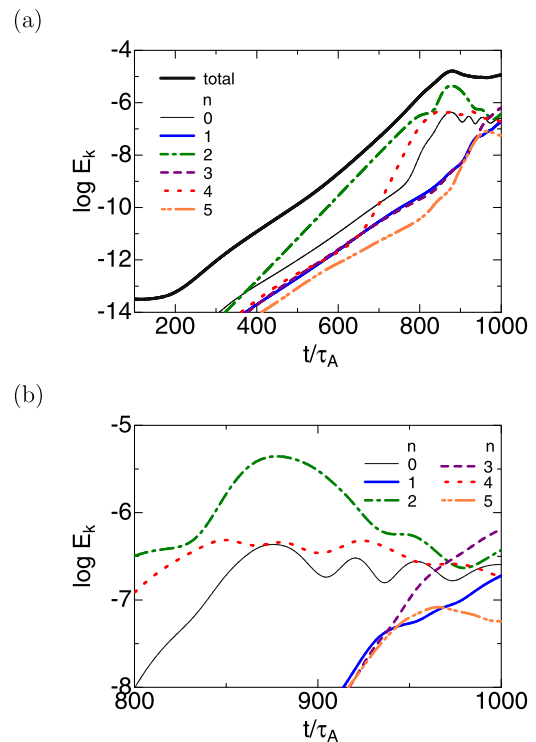


Figure 2. Time evolution of the kinetic energy for $I = 0$ and $\beta_0 = 3.3\%$, (a) total kinetic energy E_k (black thick solid line) and Fourier components of the kinetic energy E_{kn} (thin lines) in the whole time region of $100 \leq t/\tau_A \leq 1000$ and (b) enlarged figure only for E_{kn} in the time region of $800 \leq t/\tau_A \leq 1000$.

as 0.1 for the entire calculation space. The constant off-axis value by 10% is added for the equilibrium pressure to avoid the numerical divergence, which can occur due to the appearance of the negative pressure originated from the convection term in equation (5) in the small equilibrium pressure region. This added pressure is small compared to the total equilibrium pressure and does not change the equilibrium pressure gradient. Therefore, the effect on the present analysis is considered to be small.

The dissipation parameters are chosen as $\eta/\mu_0 = 4.0 \times 10^{-9}$, $\nu = \chi_{\perp} = 10^{-6}$ and $D = 10^{-3}$ for the resistivity, viscosity, perpendicular heat conductivity and density diffusivity, respectively, where μ_0 denotes the vacuum permeability. These parameters are normalized by $v_A R_0$, where v_A denotes the Alfvén velocity and R_0 denotes the major radius of the center of the simulation box. The chosen value of χ_{\perp} corresponds to $22.5 \text{ m}^2 \text{ s}^{-1}$ for the parameters of reference [3], which is a little larger than the range of the ion thermal diffusivity observed in the LHD experiments, $1 \sim 10 \text{ m}^2 \text{ s}^{-1}$. The viscosity is assumed to have a value similar to χ_{\perp} . Also, $\chi_{\parallel} = 10^3 \chi_{\perp}$ is utilized for the parallel heat conductivity, which is limited by the CFL condition [16]. We employ the resistivity that is larger by almost one order than the experimental value. However, this difference is not considered to give significant effects because the ideal mode is strongly unstable as shown in figure 1(c). A fairly large D is introduced in order to keep the numerical stability with respect to the density.

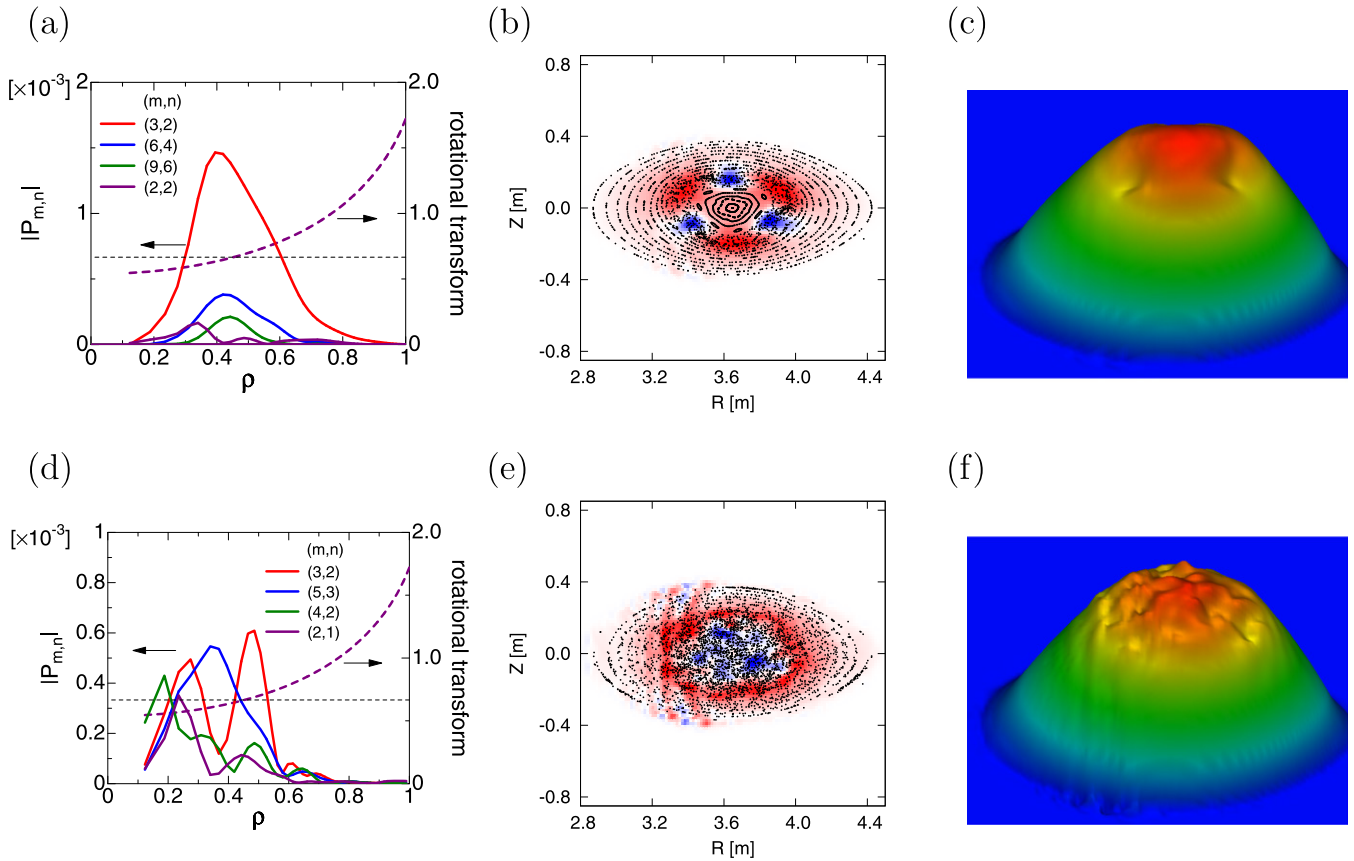


Figure 3. (a) and (d) Profiles of the largest four Fourier components of the perturbed pressure absolute value, (b) and (e) pattern of the perturbed pressure and the puncture plots of the field lines and (c) and (f) bird's eye view of the total pressure, at (a)–(c) $t = 800\tau_A$ and (d)–(f) $t = 1000\tau_A$ for $I = 0$ and $\beta_0 = 3.3\%$. Thick dashed line shows the profile of the equilibrium rotational transform in (a) and (d).

The MIPS calculation is performed in the region specified by $2.7 \text{ m} \leq R \leq 4.6 \text{ m}$, $-0.95 \text{ m} \leq Z \leq 0.95 \text{ m}$ and $0 \leq \phi \leq 2\pi$ corresponding to the full torus. The 128 grids for R and Z directions and 640 grids for ϕ direction are utilized. In the present analysis, the effect of the mode rotation is not taken into account, and therefore, the locked situation is treated.

3. Dynamics of LHD plasma without net toroidal current

First, the case without the net toroidal current ($I = 0$) with $\beta_0 = 3.3\%$ shown in figure 1 is examined as the reference. Figure 2(a) shows the time evolution of the total kinetic energy E_k which is given by

$$E_k = \frac{1}{2} \int \rho_m v^2 dV. \quad (8)$$

The Fourier component E_{kn} from $n = 0$ to $n = 5$ in the Boozer coordinates [17] corresponding to the equilibrium is also plotted, which is evaluated by

$$E_{kn} = \frac{1}{2} \int \sum_{i=R,\phi,Z} \{[(\sqrt{\rho_m} v_i)^{\cos}]^2 + [(\sqrt{\rho_m} v_i)^{\sin}]^2\} dV. \quad (9)$$

Here, the superscripts of ‘cos’ and ‘sin’ mean the cosine and the sine parts of the Fourier coefficients, respectively, and the subscript n denotes the toroidal mode number. The perturbation grows linearly up to $t \sim 750\tau_A$ and saturates nonlinearly. Here τ_A denotes the Alfvén time. In this case, the $n = 2$ component is dominant in the linear phase.

Figure 3 shows the results of the time evolution for different times, (a)–(c) for $t = 800\tau_A$ and (d)–(f) for $t = 1000\tau_A$. In figures 3(a) and (d), the absolute value of (m, n) component of the perturbed pressure defined as

$$|P_{m,n}| = [(P_{m,n}^{\cos})^2 + (P_{m,n}^{\sin})^2]^{1/2} \quad (10)$$

is plotted. As shown in figure 3(a), the (3, 2) component is localized around the $\iota = 2/3$ surface and has the Gaussian-like shape at $t = 800\tau_A$ in the early nonlinear phase. The $m = 3$ structure is seen in the perturbed pressure in figure 3(b). The magnetic surfaces are locally stochastic around the resonant surface. Also, the total pressure is deformed triangularly due to this perturbation as shown in figure 3(c). These features indicate that this mode is a typical interchange mode resonant at $\iota = 2/3$ surface.

At $t = 1000\tau_A$ in the further nonlinear evolution, several sideband components such as (5, 3), (4, 2) and (2, 1) grow as well as (3, 2) through the nonlinear coupling as shown in figure 3(d). Also as shown in figure 2(b), E_{kn} 's with different toroidal number are comparable. The

evolution of these components brings the complicated structure in the pressure perturbation and makes the field lines much more stochastic in the core region as shown in figure 3(e). Thus, the (3, 2) component is not dominant in the structure at this time anymore. According to this perturbation feature, the total pressure decays into the fine structure as shown in figure 3(f). Since the (1, 1) component is detected as the dominant component during the partial collapse in the LHD experiments, this dynamics evolution does not explain the experiments.

4. Dynamics of LHD plasma with net toroidal current

Next, the equilibrium with the net toroidal current $I/B = 29.6 \text{ kAT}^{-1}$ at $\beta_0 = 1.4\%$ shown in figure 1 is examined. Figure 4 shows the time evolution of the kinetic energy. As in the case without the net toroidal current, the linear phase appears first and is followed by the nonlinear saturation. In the linear phase, the $n = 3$ component has the largest kinetic energy and the $n = 2$ component has the second largest. However, the difference between them is small and the lines are almost overlapped in figures 4(a) and (b).

At $t = 520\tau_A$ in the early nonlinear phase, the (3, 3) component is dominant in the perturbed pressure as shown in figure 5(a). The radial profile of the (3, 3) component is close to the Gaussian type and localized around the $\iota = 1$ surface at $\rho = 0.597$. The (2, 2) component is the secondary dominant component and has the similar feature. The magnetic surfaces and the pressure structure are weakly deformed triangularly combined with the $m = 2$ effect as shown in figures 5(b) and (c). These features indicate that this mode is also a typical interchange mode as in the case without the net toroidal current.

However, at $t = 600\tau_A$ in the further nonlinear evolution, the dominant component is changed to the (2, 2) component from the (3, 3) component. The structure is localized in the core region around $\rho = 0.309$ as shown in figure 5(d). This region is apart from the resonant $\iota = 1$ surface and has a very low shear. Therefore, this mode is recognized as a non-resonant mode. Because of the convection of the vortices, the pressure and the magnetic surfaces are squeezed in the core as shown in figure 5(e). This perturbation makes the total pressure shape elongated around the axis as shown in figure 5(f).

Furthermore, at $t = 900\tau_A$, the dominant component is further changed to the (1, 1) component as shown in figure 5(g). The mode structure is also localized around $\rho = 0.368$ in the low shear core region, and therefore, the mode is still non-resonant. Therefore, as a total, the transition from the (3, 3) resonant interchange mode to the (1, 1) non-resonant mode occurs. Due to the $m = 1$ effect, the negative pressure perturbation shown by the blue pattern tends to accumulate and merge at one poloidal direction as shown in figure 5(h). As a result, the bulk part of the pressure including magnetic axis is shifted to the opposite side as shown in figure 5(i). Also as shown in figure 4(c), this transition corresponds to the situation that the $n = 1$ and $n = 2$ components becomes

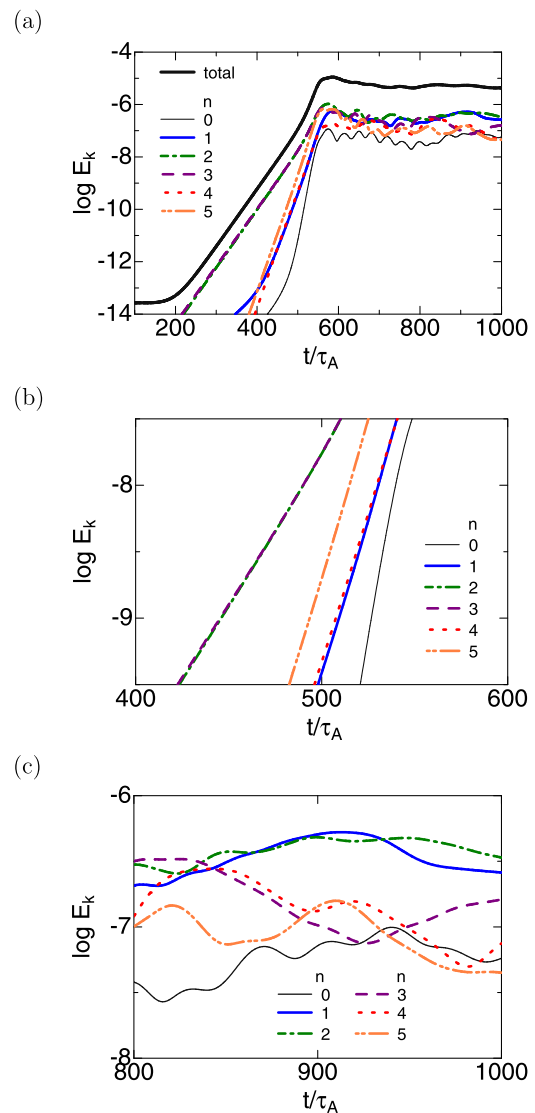


Figure 4. Time evolution of the kinetic energy for $I/B = 29.6 \text{ kAT}^{-1}$ and $\beta_0 = 1.4\%$, (a) total kinetic energy E_k (black thick solid line) and Fourier components of the kinetic energy E_{kn} (thin lines) in the whole time region of $100 \leq t/\tau_A \leq 1000$, and the enlarged figures only for E_{kn} in the time regions of (b) $400 \leq t/\tau_A \leq 600$ and (c) $800 \leq t/\tau_A \leq 1000$.

dominant in the time evolution of the kinetic energy beyond $t = 850\tau_A$.

The origin of this (1, 1) component can be understood by considering the relation of γ_n which is the growth rate of the component with the toroidal mode number n . From figure 4(b), $\gamma_{n=3} = 2.831 \times 10^{-2}$ and $\gamma_{n=2} = 2.826 \times 10^{-2}$ are obtained at $t = 500\tau_A$ in the linear phase. The sum $\gamma_{n=3} + \gamma_{n=2} = 5.657 \times 10^{-2}$ shows a good agreement with the growth rate $\gamma_{n=1} = 5.045 \times 10^{-2}$. This relation is one of the evidences that this $n = 1$ component growth is attributed to the mode coupling of the $n = 2$ and $n = 3$ components, and is not the growth of a new type of the mode different from the interchange mode. As shown in figure 5(a), which reflects the dominant components at the end of the linear phase, the dominant (m, n) components of the $n = 1, n = 2$ and $n = 3$ components

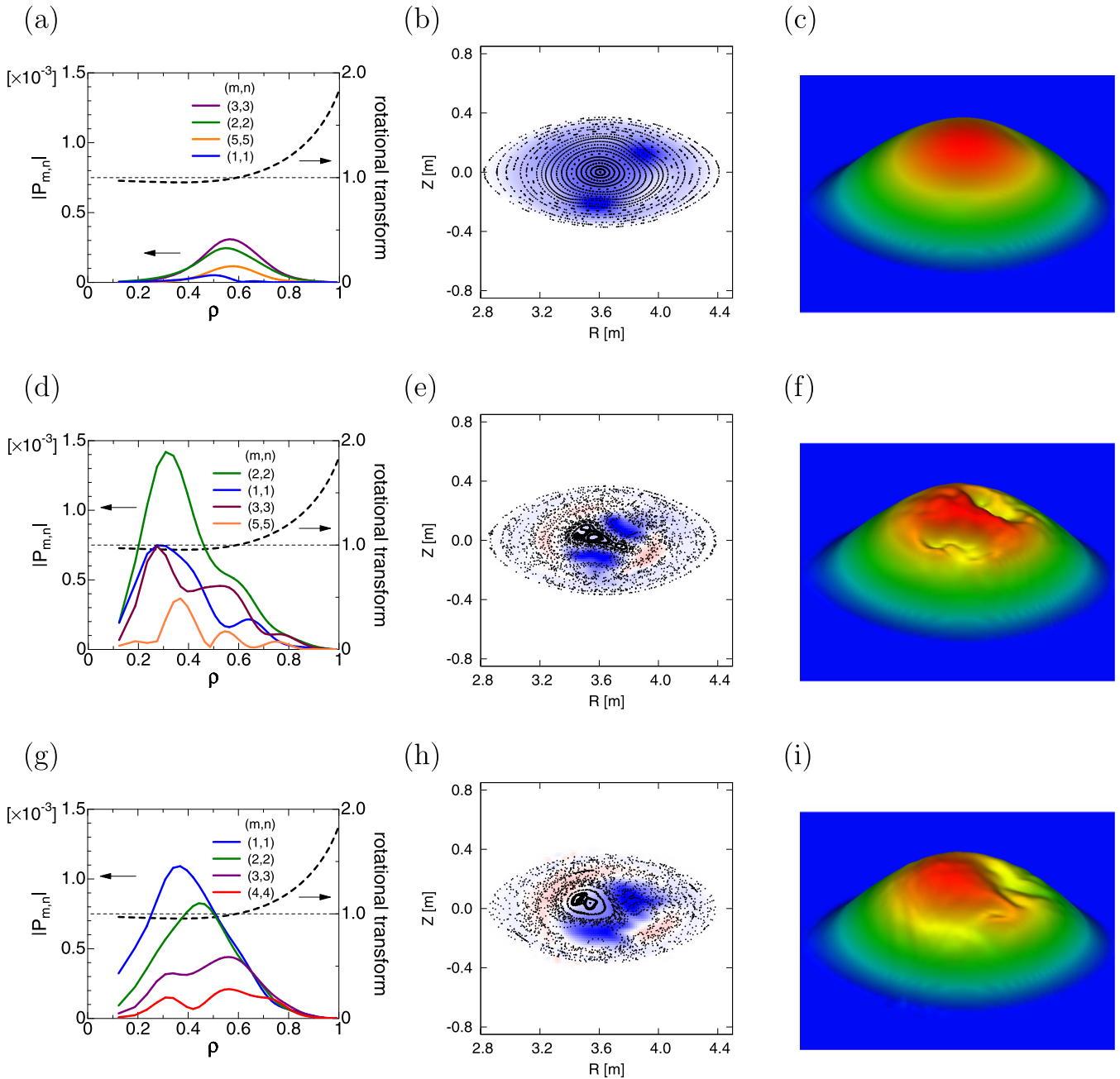


Figure 5. (a), (d) and (g) Profiles of the largest four Fourier components of the perturbed pressure absolute value, (b), (e) and (h) pattern of the perturbed pressure and the puncture plots of the field lines and (c), (f) and (i) bird's eye view of the total pressure at (a)–(c) $t = 520\tau_A$, (d)–(f) $t = 600\tau_A$ and (g)–(i) $t = 900\tau_A$ for $I/B = 29.6 \text{ kAT}^{-1}$ and $\beta_0 = 1.4\%$. Thick dashed line shows the profile of the equilibrium rotational transform in (a), (d) and (g).

are the (1, 1), (2, 2) and (3, 3) components, respectively. Therefore, we can consider that the (1, 1) component is generated by the mode coupling of the (2, 2) and (3, 3) interchange modes in the linear phase. Furthermore, in the nonlinear saturation phase, the secondary linear growth of the $n = 1$ component is not observed, which could be seen if a new type of instability would be nonlinearly generated and would grow linearly. Thus, the dominant (1, 1) component observed here is the result of the nonlinear coupling of the (2, 2) and the (3, 3) interchange modes. In other words, the (1, 1) component is not another kind of non-resonant linear instability such as

internal kink mode, infernal mode or quasi-interchange mode. The mode coupling of the (2, 2) and the (3, 3) components also generates the (5, 5) component as shown in figures 4(b) and 5(a) and (d). However, this component decays due to the viscosity and the heat conductivity, because these dissipations degrade the interchange mode with a higher mode number more effectively [18].

Figure 6 shows the time variation of the peak value of $|P_{m,n}|$ for the (1, 1), (2, 2) and (3, 3) components. The mode number of the dominant component is decreased from (3, 3) to (1, 1) continuously. The reduction of the mode numbers

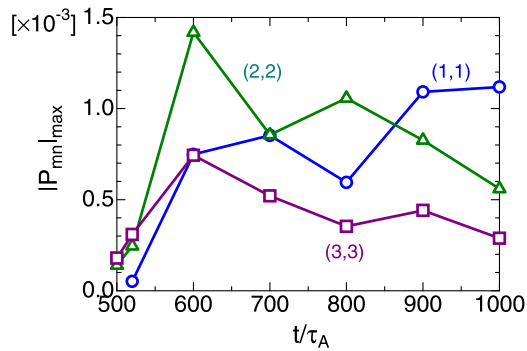


Figure 6. Time evolution of the maximum value of $|P_{mn}|$ for $(m, n) = (1, 1)$, $(2, 2)$, and $(3, 3)$ in the case of $I/B = 29.6 \text{ kA T}^{-1}$ and $\beta_0 = 1.4\%$.

in the nonlinear evolution is like an inverse cascade. This resultant dominant mode number $(1, 1)$ is observed in the LHD experiments for the partial collapses [3]. Thus, the transition obtained in this study is considered to be one of the candidates to explain the observation of the $(1, 1)$ mode in the experiments.

5. Concluding remarks

The dynamics of the LHD plasma with the net toroidal current is studied by means of the 3D numerical MHD simulations. A transition from the interchange mode resonant at the $\ell = 1$ surface to a non-resonant mode in the nonlinear evolution is found. This transition occurs in the equilibrium where the shear is weak and the rotational transform is just below unity in the core region. In the transition, the mode number of the dominant component in the pressure perturbation is decreased in the nonlinear saturation phase. This nonlinear decrease in the mode number is like an inverse cascade. In the present analysis, the mode number of the dominant component varies from $(3, 3)$ to $(1, 1)$. The profile of the perturbed pressure shows that this mode is non-resonant, because the mode is localized in the region with the low shear and apart from the $\ell = 1$ resonant surface. The total pressure profile shows the structure corresponding to the dominant $m = 1$ component after the transition. The dominant mode number $(1, 1)$ as a result of the transition is observed in the LHD experiments for the partial collapses. Thus, the transition to the $(1, 1)$ component can be one of the candidates to explain the $(1, 1)$ mode appearance in the collapse phenomena observed in the experiments.

On the contrary, such a transition does not occur in the equilibrium without the net toroidal current and with the high shear rotational transform. In this case, the standard interchange mode linearly grows. And then, many side-band components with comparable amplitude appear simultaneously in the nonlinear evolution. Such growth of many components makes the shape of the total pressure complicated. This evolution is quite different from that of the above transition to the non-resonant mode. The difference between these equilibria indicates that the low shear core region with the rotational transform close to unity is necessary for the transition.

In the variation of the mode number, there exists the similarity with the simulation of the quasi-interchange mode in the sawtooth crash [8]. In the sawtooth case, both $(1, 1)$ and $(2, 2)$ components have comparable magnitude in the beginning of the event. As the mode grows, the $(1, 1)$ component becomes to behave dominantly, which indicates the smaller mode number. The existence of the low shear region with the rotational transform or the safety factor close to unity is common between the present and the sawtooth simulations. Thus, this feature of the rotational transform is considered to be the key issue for the variation like the inverse cascade beyond the difference of the confinement configuration. On the other hand, similar non-resonant phenomena are also observed in MAST experiments [19]. In this case, long-lived saturated instabilities appear for the plasma with a low shear safety factor just above unity. Thus, it is an interesting points to discuss the similarity and the difference in the excitation mechanism of these non-resonant modes comprehensively.





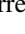
In order to understand the more detailed mechanism of the collapse phenomena, it is necessary to incorporate further physics beyond the present framework in future. One of the special features of the collapses observed in the LHD experiments is that the mode rotation frequency decreases and becomes zero just before the abrupt crash like a locked mode [3–6]. In order to analyze this property, the interaction between the plasma rotation and the instability [20] should be taken into account. It is also reported that the slowing time of the rotation frequency depends on the magnitude of the resonant magnetic perturbation (RMP) [6]. Therefore, it is desirable to include the RMP effect in the 3D equilibrium calculation [21] as well. Furthermore, Sato *et al* [22], recently showed that the effect of the kinetic ions has a stabilizing contribution to the pressure driven modes in the LHD plasma. Thus, it is also attractive to examine this effect on the transition to the non-resonant mode.

Acknowledgments

One of the authors (K.I.) thanks Professor S. Ohdachi and Dr. Y. Narushima for their fruitful discussion. This work was performed on ‘Plasma Simulator’ (NEC SX-Aurora TSUBASA) of National Institute for Fusion Science (NIFS) with the support and under the auspices of the NIFS Collaboration Research program (NIFS20KNST159) and on the JFRS-1 supercomputer system at Computational Simulation Centre of International Fusion Energy Research Centre (IFERC-CSC) in Rokkasho Fusion Institute of National Institutes for Quantum and Radiological Science and Technology (QST, Aomori, Japan). This work was partly supported by KAKENHI (15K06651, 20K03909) by Japan Society for the Promotion of Science (JSPS).

ORCID iDs

K. Ichiguchi  <https://orcid.org/0000-0002-7698-0223>
Y. Suzuki  <https://orcid.org/0000-0001-7618-6305>

Y. Todo  <https://orcid.org/0000-0001-9323-8285>
 K. Ida  <https://orcid.org/0000-0002-0585-4561>
 Y. Takemura  <https://orcid.org/0000-0003-3754-897X>
 M. Sato  <https://orcid.org/0000-0002-8921-961X>
 B.A. Carreras  <https://orcid.org/0000-0001-7921-4690>

References

- [1] Komori A. *et al* 2010 Goal and achievements of large helical device project *Fusion Sci. Technol.* **58** 1
- [2] Yamada H. *et al* 2011 Overview of results from the large helical device *Nucl. Fusion* **51** 094021
- [3] Sakakibara S. *et al* 2015 Characteristics of MHD instabilities limiting the beta value in LHD *Nucl. Fusion* **55** 083020
- [4] Takemura Y. *et al* 2017 Experimental study on slowing-down mechanism of locked-mode-like instability in LHD *Plasma Fusion Res.* **12** 1402028
- [5] Takemura Y. *et al* 2019 Study of slowing down mechanism of locked-mode-like instability in helical plasmas *Nucl. Fusion* **59** 066036
- [6] Takemura Y., Watanabe K.Y., Sakakibara S., Ohdachi S., Narushima Y., Ida K. and Yoshinuma M. 2021 External RMP effect on locked-mode-like instability in helical plasmas *Nucl. Fusion* **61** 026011
- [7] Johnson J.L., Greene J.M. and Coppi B. 1963 Effect of resistivity on hydromagnetic instabilities in multipolar systems *Phys. Fluids* **6** 1169
- [8] Sugiyama L.E., Xu L.Q. and Okabayashi M. 2021 Quasi-interchange modes and sawteeth 28th IAEA Fusion Energy Conf. (10–15 May 2021) (<https://conferences.iaea.org/event/214>) virtual event TH/P8-18
- [9] Park W., Belova E.V., Fu G.Y., Tang X.Z., Strauss H.R. and Sugiyama L.E. 1999 Plasma simulation studies using multilevel physics models *Phys. Plasmas* **6** 1796
- [10] Sugiyama L. and Park W. 2000 A nonlinear two-fluid model for toroidal plasmas *Phys. Plasmas* **7** 4664
- [11] Waelbroeck F.L. and Hazeltine R.D. 1988 Stability of low-shear tokamaks *Phys. Fluids* **31** 1217
- [12] Suzuki Y., Nakajima N., Watanabe K., Nakamura Y. and Hayashi T. 2006 Development and application of HINT2 to helical system plasmas *Nucl. Fusion* **46** L19
- [13] Todo Y., Nakajima N., Sato M. and Miura H. 2010 Simulation study of ballooning modes in the large helical device *Plasma Fusion Res.* **5** S2062
- [14] Glasser A.H., Greene J.M. and Johnson J.L. 1975 Resistive instabilities in general toroidal plasma configurations *Phys. Fluids* **18** 875
- [15] Kawamura T. and Kuwahara K. 1984 Computation of high Reynolds number flow around a circular cylinder with surface roughness *AIAA Paper* 84-0340
- [16] Courant R., Friedrichs K. and Lewy H. 1967 On the partial difference equations of mathematical physics *IBM J. Res. Dev.* **11** 215–34
- [17] Boozer A.H. 1981 Plasma equilibrium with rational magnetic surfaces *Phys. Fluids* **24** 1999
- [18] Carreras B.A., Garcia L. and Diamond P.H. 1987 Theory of resistive pressure-gradient-driven turbulence *Phys. Fluids* **30** 1388
- [19] Chapman I.T., Hua M.-D., Pinches S.D., Akers R.J., Field A.R., Graves J.P., Hastie R.J. and Michael C.A. 2010 Saturated ideal modes in advanced tokamak regimes in MAST *Nucl. Fusion* **50** 045007
- [20] Ichiguchi K. *et al* 2016 Three-dimensional numerical analysis of shear flow effects on MHD stability in LHD plasmas *Plasma Fusion Res.* **11** 2403035
- [21] Ichiguchi K., Suzuki Y., Sato M., Todo Y., Nicolas T., Sakakibara S., Ohdachi S., Narushima Y. and Carreras B.A. 2015 Three-dimensional MHD analysis of heliotron plasma with RMP *Nucl. Fusion* **55** 073023
- [22] Sato M. and Todo Y. 2020 Ion kinetic effects on linear pressure driven magnetohydrodynamic instabilities in helical plasmas *J. Plasma Phys.* **86** 815860305